Understanding inhibitor resistance in Mps1 kinase through novel biophysical assays and structures

Yoshitaka Hiruma[1], Andre Koch[2], Nazila Hazraty[1], Robbie P. Joosten[1], René H. Medema[2] and Anastassis Perrakis[1]

[1] Division of Biochemistry and [2] Cell Biology, Netherlands Cancer Institute, 1066 CX Amsterdam, the Netherlands.

Correspondence: Anastassis Perrakis, a.perrakis@nki.nl

Summary statement

The inhibition of specific Mps1 kinase inhibitors towards the wild-type protein and inhibitor-resistant mutants is explained by a novel specific activity assay, biophysical characterisation, and X-ray structures.

Short title

Mps1 C604Y and inhibitors

Keywords

X-ray crystallography, microscale thermophoresis, fluorescence polarisation, Cpd-5, NMS-P715

Abbreviation list

Mps1, monopolar spindle 1; Cpd-5, Compound-5 (N-(2,6-diethylphenyl)-8-((2-methoxy-4-(4-methylpiperazin-1-yl)phenyl)amino)-1-methyl-4,5-dihydro-1H-pyrazolo[4,3-h]quinazoline-3-carboxamide); NMS-P715, N-(2,6-diethylphenyl)-1-methyl-8-({4-[(1-methylpiperidin-4-yl)carbamoyl]-2-(trifluoromethoxy)phenyl}amino)-4,5-dihydro-1H-pyrazolo[4,3-h]quinazoline-3-carboxamide; K_D, dissociation constant; IC_{50}, half maximal inhibitory concentration; FP, fluorescence polarization; ATP, adenosine triphosphate; KNL1, kinetochore null protein 1; Bub1/Bub3, budding uninhibited by benzimidazoles 1 / budding uninhibited by benzimidazoles 3; TMR, tetramethylrhodamine; KPi, (inorganic) potassium phosphate; GST, Glutathione S-transferase; WT, wild-type; MST, microscale thermophoresis;

Abstract

Monopolar spindle 1 (Mps1/TTK) is a protein kinase essential in mitotic checkpoint signalling, preventing anaphase until all chromosomes are properly attached to spindle microtubules. Mps1 has emerged as a potential target for cancer therapy, and a variety of compounds have been developed to inhibit its kinase activity. Mutations in the catalytic domain of Mps1 that give rise to inhibitor resistance, but retain catalytic activity and do not display cross-resistance to other Mps1 inhibitors, have been described. Here we characterize one such mutant, the Mps1 C604Y that raises resistance to two closely related compounds, NMS-P715 and its derivative Cpd-5, but not to the well characterised Mps1 inhibitor, reversine. We show that estimates of the IC_{50} (employing a novel specific and efficient assay that utilizes a fluorescently labelled substrate) and of the binding affinity (K_D) confirm that the C604Y mutant is not resistant to reversine, but also indicate that Cpd-5 should be better tolerated than the closely related NMS-P715. To gain further insight, we determined the crystal structure of the Mps1 kinase bound to Cpd-5 at 2.2Å resolution, and compare the binding modes of Cpd-5, NMS-P715 and reversine bound to Mps1. The difference in steric hindrance between Tyr604 and the trifluoromethoxy moiety of NMS-P715, the methoxy moiety of Cpd-5, and complete absence of such a group in reversine, account for differences we observe *in vitro*. Our analysis enforces the notion that inhibitors targeting Mps1 drug-resistant mutations can emerge as a feasible intervention strategy based on existing scaffolds, if the clinical need arises.

Introduction

One of the common features of solid human tumors is presence of abnormal number of chromosomes, a state often referred as "aneuploidy" [1]. Previous studies indicate that a mechanism that sustains aneuploidy in tumour cells is the over-expression of high levels of monopolar spindle 1 (Mps1) kinase [2]. Mps1, also known as threonine and tyrosine kinase (TTK), is a dual specificity protein kinase, essential for safeguarding proper chromosome alignment and segregation during mitosis [2]. Due to its importance for the viability of tumor cells, Mps1 kinase has become a potential target for cancer treatment [2]. Over the past years, several dozens of small compounds have been developed to inhibit the Mps1 kinase activity [2–6]. Recently, NMS-P715 has been described to suppress the growth of medulloblastoma cells, a common malignant brain tumor in children [7]. The anti-proliferative activity of NMS-P715 has been also shown in breast, renal and colon cancer cell lines [8]. A derivative of NMS-P715, Compound 5 (Cpd-5) [9], has been reported to display higher potency towards Mps1 than NMS-P715 [10]. Although these Mps1 inhibitors have promising results in pre-clinical studies [4,7,8], they also have innate problems as kinase inhibitors [10,11]. After the initial drug response, tumor cells frequently acquire resistance and become insensitive to treatment [10,12]. The development of drug resistance in cancer cells is often the consequence of mutations of the targeted kinases [13]. These mutations are typically found in the ATP binding pocket, which renders the binding of inhibitors suboptimal, while retaining kinase activity [14]. A mutation at Cys604 of the Mps1 kinase has been isolated by raising resistance against a number of inhibitors including NMS-P715 [11] as well as Cpd-5, in cell studies [10]. It is positioned in the "hinge loop" region of the kinase domain, which is part of the ATP binding pocket [2]. Gurden *et al.* described the isolation of the C604W mutant [11], and a C604Y mutation has been independently described by Koch *et al.*, raising resistance to Cpd-5 [10]. A crystal structure of

the Mps1 kinase C604W mutant bound to NMS-P715 [11] showed how this mutation prohibits efficient binding of NMS-P715, suggesting that further development of NMS-P715 derivatives could prove necessary to combat tumor cells conferring drug resistances.

Drug development against kinases can be made more efficient by the availability of automatable direct-readout specific assays, which can be implemented in common laboratory equipment. To detect Mps1 kinase activity *in vitro*, the myelin basic protein (MBP) is widely employed as a substrate, using radiolabelled ATP or specific phospho-Mps1 antibodies [15–17]. Alternatively, the KNL1 protein is used as substrate [10], which is a well-documented Mps1 substrate of kinetochore components [18,19]. These assays are highly specific for Mps1, but hard to quantify. Another more recently demonstrated way of measuring Mps1 kinase activity is a mobility shift assay described by Naud *et al* [5]: phosphorylated and non-phosphorylated peptides are separated by electrophoresis based on their charges [13]. This mobility shift assay has been compared with a radiometric assay and found to be more robust [20].

Here, we first describe a novel and highly specific assay for Mps1 activity by using fluorescence polarization (FP), which is based on the change of tumbling rate of a fluorescently-labelled KNL1 peptide, monitoring the binding of the 73 kDa Bub1/Bub3 complex as a high-throughput highly specific physiological readout. Using this assay, we determined the IC_{50} of NMS-P715 and Cpd-5 for the Mps1 WT and C604Y mutant, and compare it to the K_D against these Mps1 variants. We also present the crystal structure of the Mps1 kinase domain bound to Cpd-5, and discuss the structural basis of the inhibition mode of Cpd-5 over NMS-P715 in the Mps1 C604Y/W mutants, and how differences between the binding modes of related inhibitors could be exploited in therapy.

Materials and Methods

Protein production

The plasmid containing a construct of the Mps1 kinase domain (residues 519−808) was a gift from Dr. Nicola Burgess-Brown (Addgene plasmid # 38907) [21]. The Mps1 kinase domain C604Y mutant was produced as previously described [22].

The pFastBac plasmid containing the GST-tagged full-length Mps1 was a gift from Dr. Geert Kops (Hubrecht Institute, Utrecht, the Netherlands). Recombinant baculovirus was produced according to the Bac-to-Bac protocols (Invitrogen). *Spodoptera frugiperda* (Sf9) insect cells were infected with the baculovirus and allowed to grow for 72 hours at 27 °C. Cells were harvested by centrifugation and re-suspended in 50 mL of 20 mM KP_i, pH 7.5, 150 mM KCl and 1 mM TCEP (buffer A) supplemented with one tablet of Pierce™ Protease Inhibitor Tablets EDTA-free (Thermo Fisher Scientific). Samples were stored at –20°C before proceeding to purification. The re-suspended cells were defrosted at room temperature and lysed by sonication for 1 min at 50% amplitude in a Qsonica Sonicator Q700 (Fisher Scientific). Following centrifugations at 21000 *g* for 20 minutes at 4 °C, the supernatant was loaded on Glutathione Sepharose 4B (GE Healthcare). After extensive washing in buffer A, the protein was eluted in buffer A supplemented with 10 mM GSH. The sample was then loaded on a Superdex G75 16/60 HiLoad (GE Healthcare) pre-equilibrated in 20 mM HEPES/NaOH, 50 mM KCl, and 3 mM DTT. The protein fractions were pooled together and concentrated to ~10 µM. The concentration of the GST-Mps1 full length was determined by absorption spectrophotometry at 280 nm, with calculated $\varepsilon = 122.8\ mM^{-1}\ cm^{-1}$. The purified protein was aliquoted and stored at –80°C.

Bub1 (residues 1−280) and Bub3 were produced as previously described [18], with modifications. The baculovirus with the Bub1 and Bub3 construct was a gift from Dr. Geert Kops. Sf9 insect cells were infected and allowed to grow for 72 hours at 27 °C. The cell cultures were harvested by centrifugation and re-suspended in 50 mM Tris/HCl, pH 7.7, 1 mM TCEP and 0.05% Tween20 (buffer B) supplemented with 300 mM KCl, 10 mM imidazole and one tablet of Pierce™ Protease Inhibitor Tablets EDTA-free (Thermo Fisher Scientific). Samples were stored at –20°C before proceeding to the purification. The re-suspended cells were defrosted at room temperature and lysed by sonication for 1 min at 50% amplitude in a Qsonica Sonicator Q700 (Fisher Scientific). Following centrifugation at 21000 *g* for 20 minutes at 4 °C, the supernatant was loaded on a HisTrap HP column (GE Healthcare). After extensive washing in buffer B supplemented with 300 mM KCl and 10 mM imidazole, the protein was eluted with buffer B supplemented with 150 mM imidazole. The sample was then loaded on a Superdex G75 16/60 HiLoad (GE Healthcare) pre-equilibrated in a buffer B supplemented with 100 mM KCl. The protein fractions were pooled together and concentrated. The concentration of the Bub1/Bub3 complex was determined by absorption spectrophotometry at 280 nm, with calculated $\varepsilon = 101.9\ mM^{-1}\ cm^{-1}$. The purified protein was aliquoted and stored at –80°C.

Chemicals

Cpd-5 was synthesized as previously described [9]. NMS-P715 was purchased from Merck Millipore. A KNL1 peptide consisting of 31 residues (^{162}KHANDQTVIFSDENQMDLTSSHTVMITKGLK^{191}) was chemically synthesized and labelled with Tetramethylrhodamine (TMR) at the N-terminus (TMR-KNL1$_p$).

Western-blot based Mps1 kinase activity assay

100 ng of Mps1 wild type or Mps1 C604Y was incubated for 10 min at 32°C with the indicated compounds in a buffer containing 50 mM Tris-HCl pH 7.5, 100 mM NaCl, 20 mM $MgCl_2$, 1 mM DTT, 0.2 mM ATP. After this incubation, 200 ng of purified GST-KNL1-M3 was added, and the mixture was incubated for 60 min at 32°C before addition of SDS-sample buffer and boiling at 95°C for 10 min. Samples were separated by SDS-PAGE and transferred to nitrocellulose membranes, blocked with 4% bovine serum albumin (w/v) at room temperature for 0.5 hour, and incubated with primary antibody (phospho-KNL1 MELT13/17; was a kind gift from Geert Kops Ref: PMID: 25402682) at 4°C overnight. After incubation with secondary antibody (1:2000 dilution) at room temperature for 1 hour, the membranes were developed with chemiluminescence ECL reagent (Amersham) and pictures were taken with the ChemiDOC XRS+ (BioRad). Resulting images were quantified using ImageJ software.

Fluorescence-based Mps1 kinase activity assay

The Bub1/Bub3 complex was titrated to a reaction mixture containing 20 nM TMR-$KNL1_p$ and 10 nM GST-Mps1 full length variants in 20 mM HEPES/NaOH pH 7.4, 1 mM ATP, 4 mM $MgCl_2$, 200 µM TCEP and 0.05% Tween20 (buffer C) with or without 50 nM of inhibitors. The samples were incubated at room temperature in a 384 well Corning assay plate. All measurements were performed in a Pherastar plate reader (BMG LABTECH GmbH, Germany).

The excitation and emission wavelengths were 540 nm and 590 nm, respectively and fluorescence polarization (FP) was calculated. All measurements were carried out in duplicate.

To calculate the IC_{50} values, the inhibitors were titrated to a reaction mixture containing 20 nM TMR-KNL1 peptide, 200 nM Bub1/Bub3 complex and 5 nM GST-Mps1 full length variants in buffer C. The samples were incubated at room temperature overnight. Measurements were carried in duplicates. The FP values were plotted against inhibitor concentration and fitted with a standard one site model (equation 1) using non-linear regression in GraphPad Prism 6 (GraphPad Software, Inc, USA).

$$FP = \left(\frac{FP_{max} \times [c]}{IC_{50} + [c]}\right) + FP_{bg} \qquad [1]$$

where FP_{max} is maximum binding in FP; [c] is inhibitor concentration; FP_{bg} is the background FP value.

Microscale Thermophoresis

The thermophoresis measurements and data analysis were performed as previously described [22] with a slight modification. The DY-547P1 labelled samples were used at a final concentration of 20 nM in Tris buffer (50 mM Tris/HCl, pH 7.4, 150 mM KCl, 1% DMSO, 0.05% Tween20). The measurement was performed at 20% LED and 40% MST power.

Crystallization

The purified Mps1 kinase domain C604Y was co-crystallized with Cpd-5, using the sitting drop vapour diffusion method in MRC 2-Well Crystallization Plate (Swissci) UVP plates (Hampton Research), with standard screening procedures [23]. The protein solution at ~200 µM (~7.2 mg mL^{-1}) was pre-incubated with 250 µM of Cpd-5, and 0.1 µL of this solution were mixed with 0.1 µL of reservoir solution and equilibrated against a 50 µL reservoir. Crystals were obtained in

15.5% (w/v) PEG 350 MME, 10 mM $MgCl_2$, and 100 mM Tris/HCl, pH 8.8. Crystals appeared at 18 °C within 24 hours. Crystals were briefly transferred to a cryoprotectant solution containing the reservoir solution and 20% (w/v) ethylene glycol and vitrified by dipping in liquid nitrogen.

Data collection and structure refinement

X-ray data were collected on beamline ID30A-3 at the European Synchrotron Radiation Facility (ESRF). The images were integrated with XDS [24] and merged and scaled with AIMLESS [25]. The starting phases were obtained by molecular replacement using PHASER [26] with an available Mps1 structure (PDB code 3HMN) [27] as the search model. Geometric restraints for the compounds were made in AceDRG [28]. The models were built using COOT [29] and refined with REFMAC [30] in iterative cycles; at the beginning and at some stages of the procedure model re-building and refinement parameters adjustment was performed in PDB-REDO [31,32]. The quality of the models was evaluated by MOLPROBITY [33]. Data collection and refinement statistics are presented in Table 1.

Results

Cpd-5 and NMS-P715 inhibit Mps1-mediated phosphorylation of KNL1 peptides

To enable quick spectroscopic quantitation of Mps1 activity, we synthesized a fluorescent KNL1 peptide, TMR-KNL1. As shown in Figure 1A, phosphorylation of TMR-KNL1 by Mps1 can be detected specifically by the Bub1/Bub3 complex that binds only the phosphorylated form of the peptide. Bub1/Bub3 form a tight complex with TMR-KNL1, with a dissociation constant (K_D) of 12.2±1.4 nM (Figure 1B). Binding of the 73 kD Bub1/Bub3 complex reduces the tumbling rate of the ~4 kD TMR-KNL1 peptide, allowing measurement of Bub1/Bub3 binding, and therefore of phosphorylation, by fluorescence polarization (FP). Addition of the Cpd-5 or NMS-P715 Mps1 inhibitors does not notably change the binding constant of the Bub1/Bub3 complex, as expected, but only the end point measurement of the FP signal, which is proportional to the degree of phosphorylation of the peptide.

Having established the conditions for the FP assay, we measured the ability of Cpd-5 and NMS-P715 to inhibit the activity of Mps1 kinase domain on the KNL1 substrate, by titrating them into our assay mixture (Figure 2A and Table 2). From the titration curves, the IC_{50} values were estimated to be 9.2±1.6 nM for Cpd-5 and 139±16 nM for NMS-P715. Cpd-5 and NMS-P715 inhibit the C604Y variant with a significantly lower IC_{50} of 170±30 nM for Cpd-5 and 3016±534 nM for NMS-P715, respectively. To validate the result of our new assay, the potency of the inhibitors was assessed also by probing phospo-KNL1 protein with a phospho-specific antibody, which results in similar IC_{50} values (Figure 2C and Table 2). These results are fully in agreement to previous studies which showed that expression of the C604Y mutant renders cells more resistant to NMS-P715 than to Cpd-5 [10].

Binding affinities of Cpd-5 and NMS-P715 to wt and C604Y Mps1

The IC_{50} value shows how effective a compound is on a specific assay, but it is not a measurement of the binding of the inhibitor; the latter information is important to understand from a mechanistic perspective the action of inhibitors and the differential effect they assert to mutant proteins. Thus, to evaluate the influence of the C604Y substitution in the inhibition mode, the binding affinities were determined by microscale thermophoresis (MST; Figure 2B and Table 2). The MST results show that Cpd-5 binds approximately 300 fold better to the wild-type Mps1 (1.6±0.2 nM) than to the C604Y mutant (471±50 nM); a similar trend is observed for NMS-P715, which binds approximately 375 fold better to the wild-type Mps1 (4.7 ± 2.5) than to the C604Y mutant (1764±204 nM). Notably however, despite the significant reduction in binding affinity to the C604Y mutant, Cpd-5 binds four fold better than NMS-P715. This observation is consistent with the IC_{50} measurements *in vitro* and with cell-based assays [10], where Cpd-5 shows 5-15 times higher potency than NMS-P715 towards inhibiting the C604Y mutant. This is of potential interest for the discovery of compounds that target resistant variants of the kinase, and is important in light of our crystallographic structure of Cpd-5 bound to the C604Y mutant.

Crystal structure of the Mps1 kinase domain bound to Cpd-5

The Mps1 kinase domain C604Y mutant was co-crystalized with Cpd-5. The crystal structure was determined by molecular replacement, at 2.2 Å resolution. There was clear electron density for Cpd-5 in the ATP-binding pocket (Figure 3A−C) that is unusually deep in the Mps1 kinase. The overall structure of the protein adapts to a conformation very similar to the previously reported structures [2]. As in many structures of Mps1, the activation loop encompassing residues 676−685 had poor density and has not been included in the model. Thr686 in the P+1

loop has been shown to be auto-phosphorylated in the recombinant protein [2]; although we tried to model the phosphoryl group of Thr686, it is not well resolved in the electron density map and therefore it has not been included to the structural model. Interestingly, the electron density of a polyethylene glycol molecule, which sometimes encapsulates the catalytic Lys553 due to the crystallization conditions [2], is not present in our data. In our Cpd-5 bound structure, similar to the NMS-P715 complex structure, the side chain of Lys553 forms a hydrogen bond to the O atom adjacent to the diethyl phenyl ring of Cpd-5. Cpd-5 is stabilized by two additional hydrogen bond interactions with the amide backbone of the "hinge loop" residue, Gly605.

We then compared the interaction of Cpd-5 to Mps1 C604Y, with that of NMS-P715 bound to Mps1 C604W (PDB: 5AP7) [11]. The structure of Mps1 C604W was first re-evaluated with PDB_REDO to result in a model and an electron density map created with the same methodology as for our current structure. The overall binding mode of Cpd-5 was found to be very similar to that of NMS-P715 (Figure 3D−F). The electron density of the Cys604 point mutation is clearly resolved in both structures, indicating that the side chains of the substituted Tyr and Trp are well ordered in place. Despite the similar resolution of the NMS-P715 structure (2.45 Å), the orientation of the methylpiperidine moiety is not as well resolved in the electron density map as the methylpiperazine moiety in the Cpd-5 structure. This can be explained by the crystal contact with Thr509, which is poorly ordered. This difference could also be regarded as an artefact of crystallisation rather than a difference in binding mode. The key difference between the two inhibitors is the functional group of the methoxyphenyl moiety. The trifluoromethoxy group of NMS-P715 is positioned at close proximity to the side chains of Trp604 and Ile531. It is reasonable to assume that the two orders of magnitude reduction of the binding affinity is attributed to the increasing chances of steric hindrance between Trp604/Ile531 and this trifluoromethoxy moiety. The methoxyphenyl moiety of Cpd-5 is also

positioned in the vicinity to Tyr604. However, the absence of the three fluorine atoms in the functional group reduces the steric hindrance, which results in shifting the position of Cpd-5 towards Tyr604. It is interesting to note that one of the fluorines in NMS-P715 makes a close contact with the $H\varepsilon_1$ of Trp604 (2.3Å) and an even closer contact to the $H\varepsilon_{21}$ of Gln541 (2.0Å). Particularly the latter close contact can be regarded as a good example of rare hydrogen bonds of the C-F•••H-N type [34]. The χ3-torsion angle of Gln541 changes by 30 degrees to accommodate this interaction in the Trp604 mutant compared to the Tyr604 mutant. However in the Tyr604 mutant a hydrogen bond between Hε21 of Gln541 and the side-chain oxygen of Tyr604 is available (as is observed in the Cpd-5 structure) and energetically favourable. This means that both favourable interactions between fluorine in NMS-P715 and the protein are unavailable in the Tyr604 mutant. Modelling Tyr604 in the C604W:NMS-P715 structure model, using the same conformation as in our Cpd-5 structure, suggests that the trifluoromethoxy moiety would clash with the Tyr604 side chain, forcing the ligand in a different, less favourable, binding pose. This structural comparison analysis explains the difference of K_D and IC_{50} between Cpd-5 and NMS-P715 in the Mps1 C604Y variant.

Discussion

Over the past years, the Mps1 kinase has become a potential target for cancer therapy and an increasing number of Mps1 inhibitors has been published and patented [2]. However, recent reports expectedly suggest that the mutations in Mps1 confer drug resistances in tumor cells [10,11]. To combat aggressive tumor cells, further development of Mps1 inhibitors is necessary; yet this has been hindered by labour-intensive assays. Here, we describe a novel fluorescence-based Mps1 kinase assay, which allows us to measure the potency (IC_{50}) of inhibitors more efficiently than conventional methods. Using this assay, and comparing with conventional methods as well as to the actual affinity (K_D) of the compounds towards wild-type and C604Y Mps1, we find that binding of NMS-P715 is more affected than Cpd-5. This observation, consistent with cell studies showing that the C604Y substitution confers resistance more moderately to Cpd-5 than to NMS-P715 [10], indicates that combinations of different Mps1 inhibitors can be used to avoid or combat resistance in the clinic, and molecular understanding of the Mps1 interaction with inhibitors is important.

The molecular basis of the non-resistant phenotype of the C604Y mutant towards reversine [10] is supported by measurement of reversine affinity to wild-type and C604Y Mps1 (Figure 4A and Table 2); the affinity of reversine to both Mps1 variants is the same within error. Comparison of the structure of the C604Y mutant bound to reversine (PDB: 5LJJ, [22]) clearly shows why reversine can be accommodated with the same affinity in both Mps1 variants (Figure 4B), as there is no steric hindrance with the Tyr604 side chain.

To understand the molecular details behind the potency of Cpd-5 towards wild-type and C604Y Mps1, we determined the crystal structure of the C604Y variant bound to Cpd-5. Cpd-5 binds to the ATP binding pocket of the Mps1 kinase in a manner similar to NMS-P715. Yet, comparison

of the structures of Cpd-5 and NMS-P715 bound to the C604Y and C604W mutant respectively, indicates that the size of the methoxy functional group of the terminal phenyl moiety plays a key role in the steric hindrance with the bulky side chain of Tyr/Trp604. At the same time we observed that different favourable interactions between the methoxy group substitutions and the protein exist. We suggest that substitutions of the methoxy group could be used to develop perhaps less potent Mps1 inhibitors, that could be used to target the 604 mutation, if the need arises in the clinic. For instance, inhibitors for the Trp604 mutant may benefit from a single or a double fluorine substitution on the methoxy group rather than the triple substitution in NMS-P715.

Our study contributes in understanding the mechanism of resistance in Mps1 kinase inhibitors, suggests a new efficient and specific assay to aid Mps1 inhibitor discovery, and put forwards novel design principles for the further development of this class of inhibitors.

Acknowledgements

We thank Prof. Dr. Geert Kops for the many discussions about Mps1 kinase and his support. We thank the ESRF for their support, in particular beamline scientist David von Stetten, at beamline ID30A-3.

Declaration of Interest

There are no competing interests

Funding information

This work was financially supported by the Netherlands Organization for Scientific Research (NWO) (by Veni grant 722.015.008 to YH and by Vidi grant 723.013.003 to RPJ) and by KWF grant 2012-5427 to AP and Prof. Dr. Geert Kops.

Author contribution statement

YH performed or participated in all experiments; AK performed the antibody-based Mps1 activity experiments; NH helped in establishing and performing the FP experiments; RPJ helped in structure refinement and analysis; RHM and AP supervised experiments; this work was initiated by AK and YH; YH and AP wrote the paper with help from all authors.

References

1 Lengauer, C., Kinzler, K. W. and Vogelstein, B. (1997) Genetic instability in colorectal cancers. Nature **386**, 623–627.

2 Liu, X. and Winey, M. (2012) The MPS1 family of protein kinases. Annu Rev Biochem **81**, 561–585.

3 Lan, W. and Cleveland, D. W. (2010) A chemical tool box defines mitotic and interphase roles for Mps1 kinase. J Cell Biol **190**, 21–24.

4 Maia, A. R., de Man, J., Boon, U., Janssen, A., Song, J. Y., Omerzu, M., Sterrenburg, J. G., Prinsen, M. B., Willemsen-Seegers, N., de Roos, J. A., et al. (2015) Inhibition of the spindle assembly checkpoint kinase TTK enhances the efficacy of docetaxel in a triple-negative breast cancer model. Ann Oncol **26**, 2180–2192.

5 Naud, S., Westwood, I. M., Faisal, A., Sheldrake, P., Bavetsias, V., Atrash, B., Cheung, K.-M. J., Liu, M., Hayes, A., Schmitt, J., et al. (2013) Structure-Based Design of Orally Bioavailable 1 *H* -Pyrrolo[3,2- *c*]pyridine Inhibitors of Mitotic Kinase Monopolar Spindle 1 (MPS1). J. Med. Chem. **56**, 10045–10065.

6 Innocenti, P., Woodward, H. L., Solanki, S., Naud, S., Westwood, I. M., Cronin, N., Hayes, A., Roberts, J., Henley, A. T., Baker, R., et al. (2016) Rapid Discovery of Pyrido[3,4-d]pyrimidine Inhibitors of Monopolar Spindle Kinase 1 (MPS1) Using a Structure-Based Hybridization Approach. J. Med. Chem. **59**, 3671–88.

7 Alimova, I., Ng, J., Harris, P., Birks, D., Donson, A., Taylor, M., Foreman, N., Venkataraman, S. and Vibhakar, R. (2016) MPS1 kinase as a potential therapeutic target in medulloblastoma. Oncol. Rep. **36**, 2633–2640.

8 Colombo, R., Caldarelli, M., Mennecozzi, M., Giorgini, M. L., Sola, F., Cappella, P., Perrera, C., Depaolini, S. R., Rusconi, L., Cucchi, U., et al. (2010) Targeting the Mitotic Checkpoint for Cancer Therapy with NMS-P715, an Inhibitor of MPS1 Kinase. Cancer Res. **70**, 10255–10264.

9 Marco, Marina, C., Mauro, A., Riccardo, C., Teresa, D., Stefano, N., Helena, P., Matteo, S. and Silvagni. (2009) Pyrazolo-quinazolines; WO2009156315 A1.

10 Koch, A., Maia, A., Janssen, A. and Medema, R. H. (2016) Molecular basis underlying resistance to Mps1/TTK inhibitors. Oncogene **35**, 2518–2528.

11 Gurden, M. D., Westwood, I. M., Faisal, A., Naud, S., Cheung, K. M., McAndrew, C.,

Wood, A., Schmitt, J., Boxall, K., Mak, G., et al. (2015) Naturally Occurring Mutations in the MPS1 Gene Predispose Cells to Kinase Inhibitor Drug Resistance. Cancer Res **75**, 3340–3354.

12 Barouch-Bentov, R. and Sauer, K. (2011) Mechanisms of drug resistance in kinases. Expert Opin. Investig. Drugs **20**, 153–208.

13 Smyth, L. A. and Collins, I. (2009) Measuring and interpreting the selectivity of protein kinase inhibitors. J. Chem. Biol. **2**, 131–151.

14 Noble, M. E. M., Endicott, J. A. and Johnson, L. N. (2004) Protein Kinase Inhibitors: Insights into Drug Design from Structure. Science (80-.). **303**, 1800–1805.

15 Mattison, C. P., Old, W. M., Steiner, E., Huneycutt, B. J., Resing, K. A., Ahn, N. G. and Winey, M. (2007) Mps1 activation loop autophosphorylation enhances kinase activity. J Biol Chem **282**, 30553–30561.

16 Tyler, R. K., Chu, M. L. H., Johnson, H., McKenzie, E. A., Gaskell, S. J. and Eyers, P. A. (2009) Phosphoregulation of human Mps1 kinase. Biochem. J. **417**.

17 Kang, J., Chen, Y., Zhao, Y. and Yu, H. (2007) Autophosphorylation-dependent activation of human Mps1 is required for the spindle checkpoint. Proc. Natl. Acad. Sci. U. S. A., National Academy of Sciences **104**, 20232–7.

18 Vleugel, M., Omerzu, M., Groenewold, V., Hadders, M. A., Lens, S. M. A. and Kops, G. J. P. L. (2015) Sequential Multisite Phospho-Regulation of KNL1-BUB3 Interfaces at Mitotic Kinetochores. Mol. Cell **57**, 824–835.

19 Primorac, I., Weir, J. R., Chiroli, E., Gross, F., Hoffmann, I., van Gerwen, S., Ciliberto, A. and Musacchio, A. (2013) Bub3 reads phosphorylated MELT repeats to promote spindle assembly checkpoint signaling. Elife **2**, e01030.

20 Card, A., Caldwell, C., Min, H., Lokchander, B., Hualin Xi, Sciabola, S., Kamath, A. V, Clugston, S. L., Tschantz, W. R., Leyu Wang, et al. (2009) High-throughput biochemical kinase selectivity assays: panel development and screening applications. J. Biomol. Screen. **14**, 31–42.

21 Kwiatkowski, N., Jelluma, N., Filippakopoulos, P., Soundararajan, M., Manak, M. S., Kwon, M., Choi, H. G., Sim, T., Deveraux, Q. L., Rottmann, S., et al. (2010) Small-molecule kinase inhibitors provide insight into Mps1 cell cycle function. Nat Chem Biol **6**, 359–368.

22 Hiruma, Y., Koch, A., Dharadhar, S., Joosten, R. P. and Perrakis, A. (2016) Structural basis of reversine selectivity in inhibiting Mps1 more potently than aurora B kinase.

Proteins.

23 Newman, J., Egan, D., Walter, T. S., Meged, R., Berry, I., Ben Jelloul, M., Sussman, J. L., Stuart, D. I. and Perrakis, A. (2005) Towards rationalization of crystallization screening for small- to medium-sized academic laboratories: the PACT/JCSG+ strategy. Acta Crystallogr D Biol Crystallogr **61**, 1426–1431.

24 Kabsch, W. (2010) Xds. Acta Crystallogr D Biol Crystallogr **66**, 125–132.

25 Evans, P. (2006) Scaling and assessment of data quality. Acta Crystallogr D Biol Crystallogr **62**, 72–82.

26 McCoy, A. J., Grosse-Kunstleve, R. W., Adams, P. D., Winn, M. D., Storoni, L. C. and Read, R. J. (2007) Phaser crystallographic software. J Appl Crystallogr **40**, 658–674.

27 Chu, M. L., Lang, Z., Chavas, L. M., Neres, J., Fedorova, O. S., Tabernero, L., Cherry, M., Williams, D. H., Douglas, K. T. and Eyers, P. A. (2010) Biophysical and X-ray crystallographic analysis of Mps1 kinase inhibitor complexes. Biochemistry **49**, 1689–1701.

28 Long, F., Nicholls, R. A., Emsley, P., Gražulis, S., Merkys, A., Vaitkus, A. and Murshudov, G. N. (2017) *AceDRG* : a stereochemical description generator for ligands. Acta Crystallogr. Sect. D Struct. Biol., International Union of Crystallography **73**, 112–122.

29 Emsley, P. and Cowtan, K. (2004) Coot: model-building tools for molecular graphics. Acta Crystallogr D Biol Crystallogr **60**, 2126–2132.

30 Murshudov, G. N., Skubak, P., Lebedev, A. A., Pannu, N. S., Steiner, R. A., Nicholls, R. A., Winn, M. D., Long, F. and Vagin, A. A. (2011) REFMAC5 for the refinement of macromolecular crystal structures. Acta Crystallogr D Biol Crystallogr **67**, 355–367.

31 Joosten, R. P., Joosten, K., Murshudov, G. N. and Perrakis, A. (2012) PDB_REDO: constructive validation, more than just looking for errors. Acta Crystallogr. D. Biol. Crystallogr. **68**, 484–96.

32 Joosten, R. P., Long, F., Murshudov, G. N. and Perrakis, A. (2014) The PDB_REDO server for macromolecular structure model optimization. IUCrJ **1**, 213–220.

33 Davis, I. W., Leaver-Fay, A., Chen, V. B., Block, J. N., Kapral, G. J., Wang, X., Murray, L. W., Arendall 3rd, W. B., Snoeyink, J., Richardson, J. S., et al. (2007) MolProbity: all-atom contacts and structure validation for proteins and nucleic acids. Nucleic Acids Res **35**, W375-83.

34 Howard, J. A. K., Hoy, V. J., O'Hagan, D. and Smith, G. T. (1996) How good is fluorine as a hydrogen bond acceptor? Tetrahedron **52**, 12613–12622.

35 McNicholas, S., Potterton, E., Wilson, K. S. and Noble, M. E. M. (2011) Presenting your structures: the CCP4mg molecular-graphics software. Acta Crystallogr. D. Biol. Crystallogr. **67**, 386–94.

Table 1. Crystallographic Data

PDB identifier	5MRB
Data Collection	
Wavelength (Å)	0.97
Resolution (Å)	41.39−2.20 (2.27−2.20)
Space Group	I 2 2 2
Unit Cell a, b, c (Å)	70.58, 111.42, 115.03
$CC_{1/2}$	0.999 (0.702)
R_{merge}	0.040 (0.764)
I/σI	18.2 (1.9)
Completeness (%)	99.3 (99.8)
Multiplicity	4.6 (4.8)
Unique Reflections	23225
Refinement	
Atoms protein/ligand/other	2164/43/119
B-factors protein/ligand/other ($Å^2$)	62/53/69
R_{work}/R_{free} (%)	17.3/21.6
Bond lengths rmsZ/rmsd (Å)	0.525/0.011
Bond angles rmsZ/rmsd (^{o})	0.637/1.366
Ramachandran preferred/outliers (%)	97.7/0.4
Rotamers preferred/outliers (%)	96.7/0.8
MolProbity clash score (%-ile)	100
MolProbity score (%-ile)	100

High Resolution shell in parentheses

Table 2. Inhibition constants and affinities

IC_{50} (nM) – cells			
Inhibitors	WT	C604Y	Ratio
Cpd-5	17	320	18.8
NMS-P715	170	>2000	>10
IC_{50} (nM) – Bub1/Bub3 KNL1 FP assay			
Inhibitors	WT	C604Y	Ratio
Cpd-5	9.2 ± 1.6	170 ± 30	18.5
NMS-P715	139 ± 16	3016 ± 534	21.7
IC_{50} (nM) – αKNL1			
Inhibitors	WT	C604Y	Ratio
Cpd-5	69 ± 23	458 ± 167	7
NMS-P715	34 ± 6	1337 ± 402	39
K_D (nM) – MST			
Inhibitors	WT	C604Y	Ratio
Cpd-5	1.6 ± 0.2	471 ± 50	294
NMS-P715	4.7 ± 2.5	1764 ± 204	375
Reversine	41 ± 21	86 ± 24	2.1

Figure 1: fluorescence polarisation assay for specific Mps1 activity

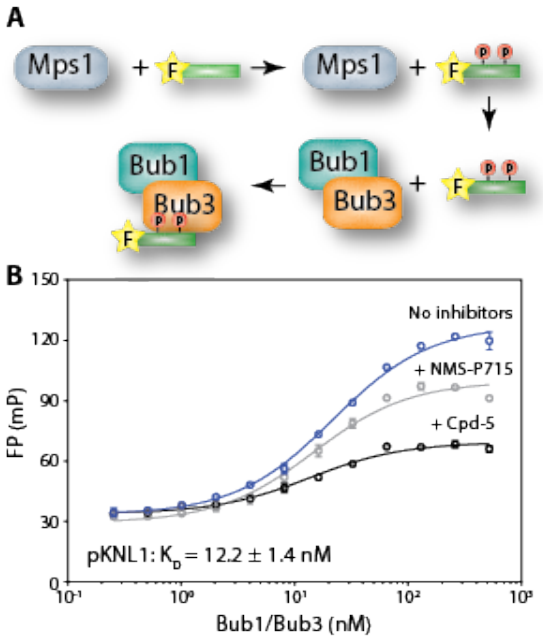

(A) the overall scheme of the FP assay; the peptide (green bar) is fluorescently labelled (yellow star) (B) FP measurements of Mps1 kinase activity (blue) by titrating the Bub1/Bub3 complex. Grey and black circles represent the measurement in the presence of NMS-P715 and Cpd-5, respectively.

Figure 2: characterisation of Mps1 C604Y mutant and inhibitors

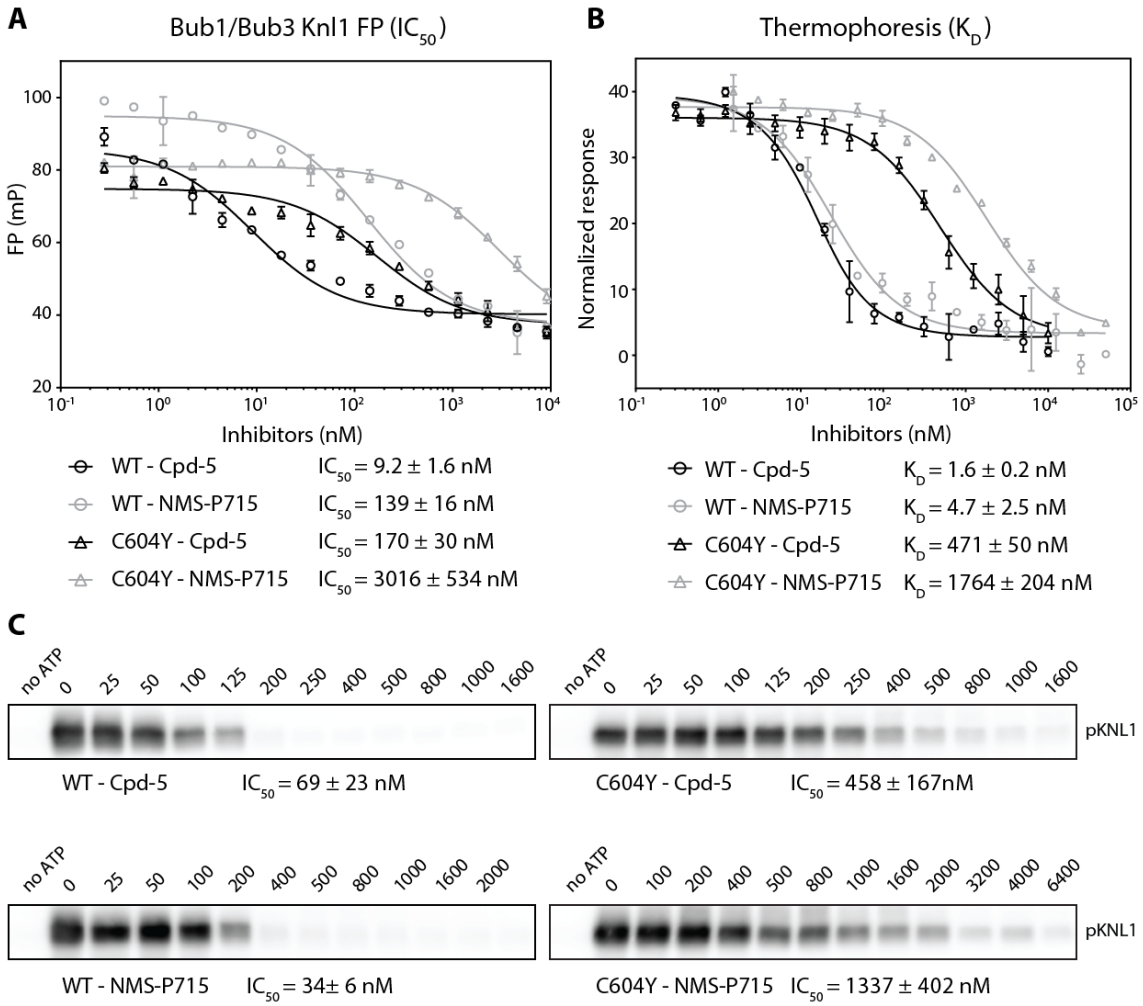

(A) FP assay for the Mps1 kinase variants in the presence of inhibitors; WT and C604Y kinase activities are shown in circles and triangles, respectively. IC_{50} values were calculated by titrating Cpd-5 (black) and NMS-P715 (grey). (B) Binding affinity measurements of the Mps1 variants with inhibitors, measured by MST. (C) IC_{50} measurements of the Mps1 kinase by probing phosphorylated KNL1 with antibodies.

Figure 3: Comparison of the Cpd5:C604Y and NMS-P715:C604W structures

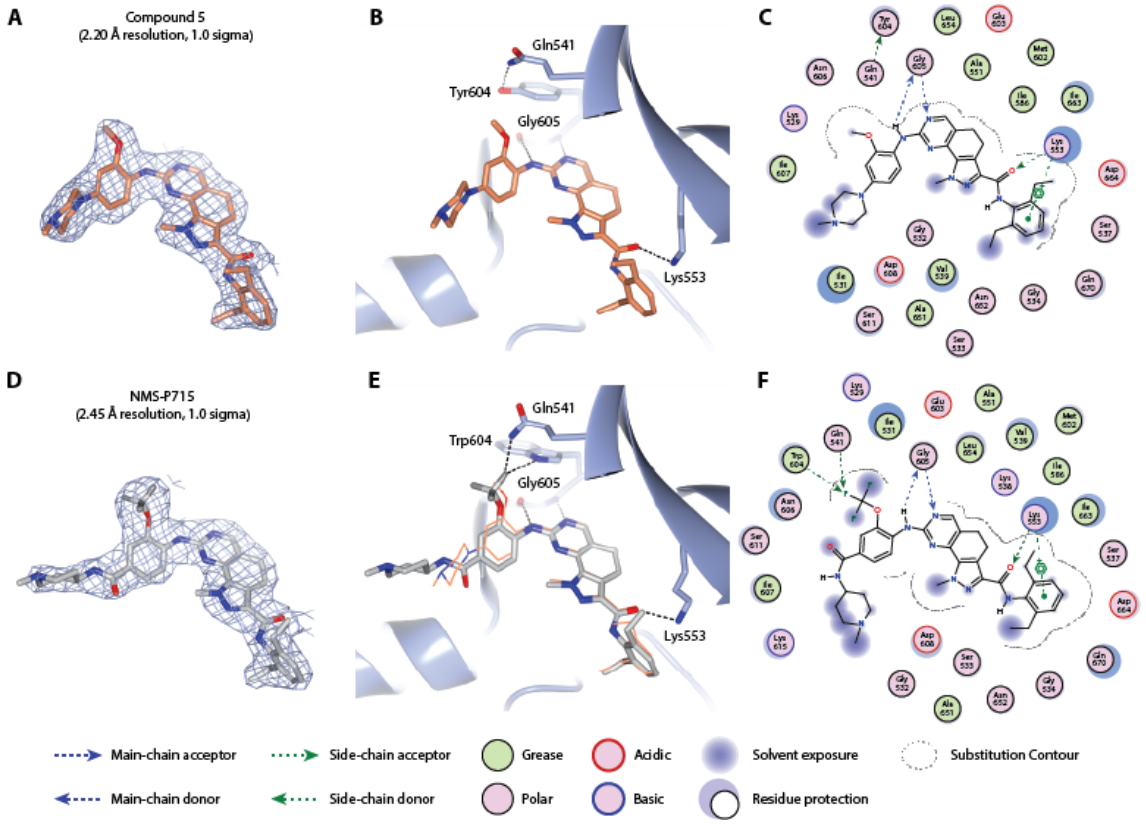

(A) $2mF_o$-DF_c electron density map of Cpd-5 in Mps1 kinase contoured at 1.0σ (carved at 2.5 Å from the Cpd-5 atoms). (B) Cpd-5 in the ATP binding pocket of Mps1 C604Y; Cpd-5, the side chain of Gln541, Tyr604 as well as Lys553 and Gly605 are depicted as sticks; hydrogen bonds are depicted as black dotted lines. Figures were made in CCP4mg [35]. (C) Cpd-5 interactions with Mps1 kinase drawn by the Lidia routine in COOT. (D, E, F) The same as A, B, C for the interaction of NMS-P715 with Mps1 C604W; in (E) Cpd-5 is shown with thin lines.

Figure 4: Comparison of the Cpd5 and reversine C604Y binding modes

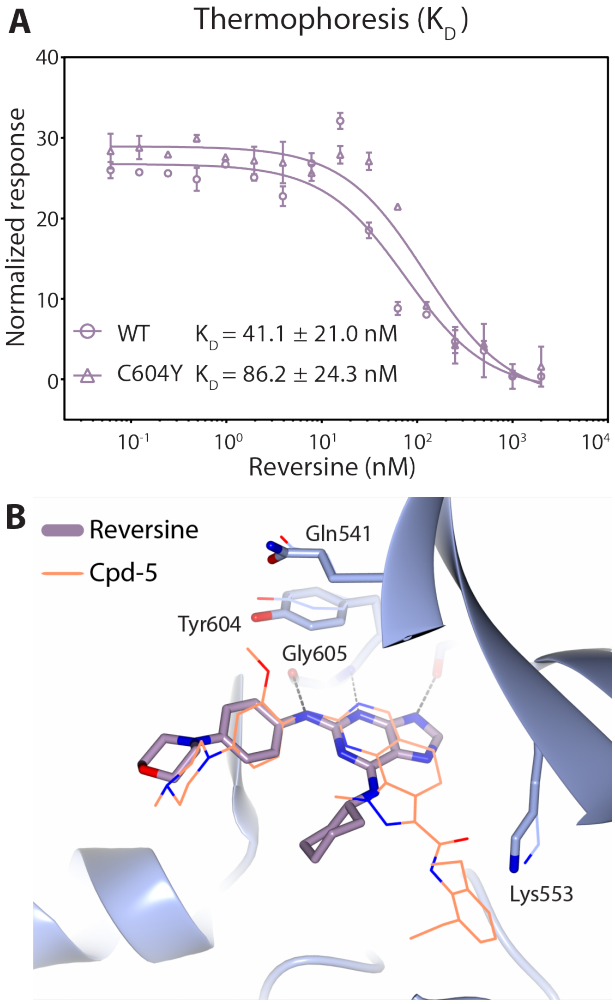

(A) Binding affinity measurements of reversine to the Mps1 variants measured by MST. (B) Reversine in the ATP binding pocket of Mps1 C604Y; Cpd-5 is shown with thin orange lines for comparison.